

MOLECULAR DYNAMICS SIMULATION OF THE M2 HELICES WITHIN THE NICOTINIC ACETYLCHOLINE RECEPTOR TRANSMEMBRANE DOMAIN: STRUCTURE AND COLLECTIVE MOTIONS

*Andrew Hung, Kaihsu Tai, and Mark S.P. Sansom**

Department of Biochemistry,
University of Oxford,
South Parks Road,
Oxford,
OX1 3QU,
U.K.

*To whom correspondence should be addressed

e-mail: mark.sansom@biop.ox.ac.uk

Tel: +44-1865-275371

Fax: +44-1865-275182

(*Biophys. J.*, ms. 2004/052878)

Note to editor: revised sections are highlighted in cyan

ABSTRACT

Multiple nanosecond duration molecular dynamics (MD) simulations were performed on the transmembrane region of the *Torpedo* nicotinic acetylcholine receptor (nAChR) embedded within a bilayer mimetic octane slab. The M2 helices and M2-M3 loop regions were free to move whilst the outer (M1, M3, M4) helix bundle was backbone restrained. The M2 helices largely retain their hydrogen-bonding pattern throughout the simulation, with some distortions in the helical-end and loop regions. All of the M2 helices exhibit bending motions, with the hinge point in the vicinity of the central hydrophobic gate region (corresponding to residues α L251 and α V255). The bending motions of the M2 helices lead to a degree of dynamic narrowing of the pore in the region of the proposed hydrophobic gate. Calculations of Born energy profiles for various structures along the simulation trajectory suggest that the conformations of the M2 bundle sampled correspond to a *closed* conformation of the channel. Principal components analyses (PCA) of each of the M2 helices, and of the five-helix M2 bundle, reveal concerted motions that may be relevant to channel function. Normal mode analyses using the anisotropic network model (ANM) reveal collective motions similar to those identified by PCA.

INTRODUCTION

The nicotinic acetylcholine receptor (nAChR) is currently the most structurally and functionally well-characterised member of the superfamily of ligand-gated ion channels (LGIC), which includes glycine, GABA and serotonin receptor-channels (Corringer et al., 2000; Karlin, 2002; Lummis, 2004). It has a pentameric structure, comprising of five subunits arranged around an approximate fivefold axis. Subtypes of nAChR are characterised by subunit composition, and are broadly divided into neuronal types (composing of homopentamers or heteropentamers of subunits α 1-10 and β 1-9), and muscle types (heteropentamers of subunits α , β , γ or ϵ , and δ). Numerous mutagenesis and labelling studies of the receptor (Lester, 1992; Karlin and Akabas, 1995; Changeux et al., 1992; Corringer et al., 2000) have established the overall topology of the transmembrane (TM) domain of the protein, identifying M2 as the pore-lining helix, shielded from the surrounding lipid environment by the M1, M3 and M4 lipid-exposed helices. More recent mutagenesis studies have explored the nature of the conformational transitions linking acetylcholine binding to the extracellular ligand binding domain (LBD) to opening of the channel formed by the TM domain (Grosman et al., 2000; Cymes et al., 2002; Lester et al., 2004).

Cryoelectron microscopy (EM) of the closed (Unwin, 1993) and open (Unwin, 1995) states of the *Torpedo* nAChR yielded 9 Å resolution images of the inner M2 helix bundle, enabling modelling and simulation studies of the M2-lined pore in relationship to channel function (Sankararamakrishnan et al., 1996; Adcock et al., 1998; Adcock et al., 2000). However, such studies were limited by the resolution of the available structural data. More recently, a higher resolution (4 Å) structure of the transmembrane domain of *Torpedo* nAChR in the closed state has been obtained (Miyazawa et al., 2003). On the basis of this structure it has been suggested that short loops between the β -strands of the LBD interact with the M2-M3 loops of the TM domain to form the main direct contact between the LBD and the pore-

lining M2 helices. It is also suggested that rotation of the inner sheets of the LBD after ligand binding is communicated through the α subunit M2-M3 loops, resulting subsequently in same-sense rotation of the α M2 helices.

The gate of the nAChR is thought to be formed by a ring or rings of hydrophobic residues close to the centre of the M2 helix bundle. A variety of experiments suggest the gate may be close to the L9' (i.e. α L251 – see Fig. 1 for M2 sequences and numbering) ring (Lester, 1992; Lester et al., 2004; Bertrand et al., 1993; Corringer et al., 2000). Model calculations suggest that such rings of hydrophobic residues can form an effective barrier to ion permeation (Beckstein et al., 2001; Beckstein and Sansom, 2003; Beckstein et al., 2003; Beckstein and Sansom, 2004; Corry, 2004; Anishkin and Sukharev, 2004). Rotation of the M2 helices is thought to open the channel by increasing the radius of the pore and/or by increasing its polarity by moving polar sidechains into the pore lining region. Rotation of only two M2 α helices is suggested to be sufficient to disrupt the hydrophobic interactions between the five-helix M2 bundle, causing the concerted collapse of the helices against the outer wall which result in pore widening by around 0.3 nm (Miyazawa et al., 2003).

Although the structural data provides vital insights, an atomic-level understanding of the gating mechanism of nAChR is currently inaccessible by experimental methods alone, although the propagation of conformational changes from the LBD to the TM domain has been studied at residue-level resolution (Grosman et al., 2000; Cymes et al., 2002). Computer simulations complement structural studies by elucidating some of the dynamical properties of the protein, and providing further clues to the dynamic mechanisms of channel activation. There have been a number of simulation studies of the TM domain components of the nAChR. Individual M2 helices, as well as M2 helix bundles, have been simulated in a variety of environments (Law et al., 2000; Law et al., 2003; Saiz and Klein, 2002; Saiz et al., 2004) to explore the dynamics of helix conformation, thus providing a complement to

functional (Oiki et al., 1988; Montal, 1995) and NMR studies of the M2 helix (Opella et al., 1999). More recently, another model of a pentameric M2 helix bundle has been proposed which appears to be consistent with NMR data on the M2 helix peptide (Kim et al., 2004). These studies have provided a detailed picture of the nature of the M2 helix bundle in isolation.

In the intact receptor, the M2 helices are shielded from direct contact with lipids, and instead are surrounded by the outer (i.e. M1, M3 and M4) helices. The interior of the pore is believed to be largely water-filled (Hille, 2001). In the current work, we seek to elucidate the influence of the environment provided by the outer helices, especially of M1 and M3, on the structure and dynamics of the pore-lining M2s. The simulation in the current work therefore serves as a first approximation to the study of M2 dynamics within the framework of a current proposed gating mechanism (Miyazawa et al., 2003), in which the outer helices act as a relatively stationary scaffold within which the M2 helices move. Additionally, we have performed normal mode analyses (NMA) on the TM domain using a coarse-grained anisotropic network model (ANM) in order to identify possible low frequency collective motions. Comparison of these motions with those extracted from the MD trajectory allows an estimate of the extent to which the atomistic simulation (which describes protein dynamics on a nanosecond timescale) was able to capture larger scale motions.

SIMULATION METHODOLOGY

The simulations were based on the deposited coordinates of the TM region of the nAChR (PDB code 1OED; see Fig. 2A). The protonation states of all titratable residues were estimated and assigned using methodologies for calculating pKa values of ionisable sidechains implemented in WHATIF (Vriend, 1990). These calculations suggested that ionisable sidechains with non-standard charge states were restricted to Glu and Asp residues,

all located in the outer scaffold helices (namely D238, E432 and E436 for chain α (A); D244 for chain β (B); E252 for chain δ (C); D238 and E432 for chain α (D); and E477 for chain γ (E)). All titratable residues in the M2 helices were predicted to be in their standard charge states at pH=7. In addition to the TM domain, the simulation cell included 1486 octanes, 15383 SPC waters, 259 Na⁺ and 266 Cl⁻ ions.

MD simulations were performed under constant particle number, pressure and temperature (NPT) conditions using the program GROMACS (www.gromacs.org) version 3.1.4 (Lindahl et al., 2001). The GROMOS96 (van Gunsteren et al., 1996) forcefield parameters were employed for all simulations. Temperature and pressure coupling were performed using the scheme described in (Berendsen et al., 1984). A constant pressure of 1 bar and pressure coupling constant = 1.0 ps was applied independently in all directions. Water, octane, and protein were coupled separately to a temperature bath at 300 K with temperature coupling constant = 0.1 ps. Electrostatic interactions were evaluated using the particle-mesh Ewald (PME) method (Darden et al., 1993; Essmann et al., 1995) with van der Waals interactions truncated at 1.0 nm. Integration time steps of 2 fs were used. Bond lengths were constrained via the LINCS algorithm (Hess et al., 1997).

Analyses of MD trajectories were performed using the GROMACS suite of programs. Secondary structure analysis employed DSSP (Kabsch and Sander, 1983). Helix bending motions were analysed using SWINK (Cordes et al., 2002). Pore radius profiles were determined using HOLE (Smart et al., 1996). Porcupine plots (Tai et al., 2001; Tai et al., 2002) of protein concerted motions were acquired using the DYNAMITE webserver (Barrett et al., 2004). Visualization of system geometries and evaluation of protein secondary structure were performed using VMD (Humphrey et al., 1996).

Born energy calculations (see below) were performed using the Adaptive Poisson-Boltzmann Solver (APBS) program (Baker et al., 2001), for which computational parameters

were defined as follows: partial charges and radii for the protein atoms were assigned using the PDB2PQR web server (Dolinsky et al., 2004) based on the parameters of the AMBER force field (Cornell et al., 1995), dielectric constants for water and protein were defined to be 78.5 and 2 respectively, with the system temperature set at 300 K. The ionic strength was that of a 150 mM 1:1 electrolyte, NaCl. The Born radius of the Na^+ test ion placed at various points within the pore was defined to be 0.169 nm (Rashin and Honig, 1985). The cell size dimensions around the protein were $10 \times 10 \times 10 \text{ nm}^3$.

Normal mode analyses (NMA) were performed within the approximation of the anisotropic network model (ANM). In this approach (Bahar et al., 1997; Atilgan et al., 2001), each residue of the protein is represented by the corresponding Ca atom, and interacts only with those other residues residing within a specified cut-off radius, r_C . The potential between each interacting residue pair is described by a Hookean function, with the sole parameter being the force constant γ , which is taken to be identical for all inter-residue interactions. In the present work, r_C was defined to be 1.4 nm, while γ was defined as $4.18 \text{ kJ mol}^{-1} \text{ nm}^{-2}$. In all of the NMA performed, the M4 helices (each of which is unattached to the rest of its corresponding subunit) were removed, as their inclusion resulted in large and unphysical fluctuations which are unlikely to be present in the complete, intact receptor.

RESULTS AND DISCUSSION

Simulation System

The simulation system was generated by embedding the nAChR TM domain (Fig. 2A) in a membrane mimetic octane slab with an initial z-directional thickness of 3 nm (Fig. 2B). The regions above and below the octane slab, corresponding to the extra- and intracellular faces respectively, were subsequently solvated with simple point charge (SPC (Berendsen et al., 1981)) water molecules. Water and octane molecules were equilibrated

during a 1 ns MD run with positional restraints (force constant $1000 = \text{kJ mol}^{-1} \text{ nm}^{-2}$) on all non-H protein atoms. Preliminary studies showed that in the absence of any restraints, there was large scale structural drift of the outer helices that disrupted the integrity of the TM domain. In particular, the C α RMSDs of the M4 helices rose to ~ 5.5 nm and of the M1 and M3 helices to ~ 3 nm within 1 ns. This is perhaps not surprising given the absence of the two extramembraneous domains (i.e. the LBD N-terminal to helix M1, and the intracellular domain located between helices M3 and M4) from the current model. Thus, a 10 ns ‘production’ trajectory was generated with positional restraints on the backbone atoms of the M1, M3 and M4 helices. The M2 helices, as well as the M2-M1 and M2-M3 linker loops were free to undergo unrestrained motions.

Conformational Drift and Residue Flexibility

The M2 helices remain reasonably stable during the course of the simulation, undergoing little structural drift as evidenced by the formation of a plateau after approximately 4 ns in the root-mean-square deviation (RMSD) plot of the C α atoms of all unrestrained segments (Fig. 3A, black line). Decomposition of the total RMSD into contributions from the individual subunits (coloured lines, Fig. 3A) reveals the approximate order in which the subunits attain structural stability. The RMSDs of chains B to E each exhibit a single stepwise increase between 1 and 3 ns, while chain A exhibit a relatively large stepwise increase at ~ 4 ns which is responsible for the minor “bump” in the total RMSD at the same time. The behaviour of the total and subunit-specific RMSD, and in particular their tendency to undergo single, discrete increases during the run, may be explained by analysis of their secondary structure using DSSP with respect to simulation time (data not shown). The H-bonding patterns of the M2 helices are largely retained during the trajectory, apart from some disruption at the C-termini ends of the M2 from the B(β subunit) and C (δ subunit) chains, with more significant uncoiling at the C-termini of M2 A (α), D (α) and E (γ).

Additionally, there is an uncoiling of a single helical turn at the C-terminus of the M2 of chain A (α) at approximately 4 ns, and collapse of this M2-M3 loop against the M1. Thus, the RMSD plots and DSSP analyses both suggest that the M2 bundle has apparently settled into a local energy minimum in conformational space after roughly 4 ns of simulation, and for the purposes of current analyses the trajectory is assumed to be stable between 4 ns and 10 ns.

The relative flexibility of various portions of the M2 helices are the M2-M3 loops is revealed by the root-mean-square fluctuations (RMSF) plot of the unrestrained segments (Fig. 3B) averaged over the last 5 ns of the trajectory. The highest flexibility is exhibited by the loops connecting the M2 helices to the outer scaffold, especially the M2-M3 loops. It is noteworthy that the M2-M3 loops of chains A and D (the two α subunit M2s) exhibit the highest fluctuations of the entire bundle. This may reflect a requirement for their flexibility in transmitting structural changes at the ligand binding sites to the α M2s after ligand binding. Furthermore, fluctuations in the M2-M3 loops are shown to be correlated with rotations and bending motions of the M2 helices, which in turn have an impact on the pore dimensions, as discussed below.

We have determined the relative flexibility of the TM and extramembranous domains of the protein via calculation of block averaged mean square-fluctuation (MSF) plots (Faraldo-Gómez et al., 2003; Faraldo-Gómez et al., 2004) taken for the last 5 ns of the simulation for the M1-M2, M2-M3, and M2 helical regions of the combined bundle (Fig. 3C). This analysis demonstrates that the M2-M3 loops exhibit the highest overall flexibility, followed by the M1-M2 loops, and finally the relatively rigid M2 TM helix regions. The plateau of the MSF plots after time windows of 2.5 ns suggests that the motions of the unrestrained regions of the protein are reasonably well converged, and thus the structures sampled within the trajectory during this simulation time lie within a local minimum on the

energy surface. Examination of the MSF plots for the individual subunits (data not shown) confirms that the highest fluctuations are for the M2-M3 loops of the α subunits.

M2 Helix Kink and Swivel

Inspection of the conformations of the M2 helices during the trajectory revealed several structural characteristics which differ markedly from that of the initial crystal structure (Fig. 4A). The overall α -helical structure is maintained within the timescale of the trajectory, as evidenced by analysis using DSSP (discussed above). However, all of the helices exhibit a more significant kink (bending) compared to that of the initial EM-acquired structure, with a hinge point near the pore centre. This is in qualitative agreement with the results of earlier MD simulations of isolated M2 helices (Law et al., 2000) which revealed a propensity of M2 for helix bending in the same region. It also correlates nicely with the results of Φ -value analysis (Cymes et al., 2002) which are indicative of bending and/or swivelling around a residue in the centre of M2. Kinked M2 helices have been included in a number of earlier models of the nAChR pore (e.g. (Tikhonov and Zhorov, 1998))

The nature of the M2 helix hinge-bending motion in the simulation was quantified using methods developed to analyse proline-induced hinges in TM helices (Cordes et al., 2002; Bright et al., 2002). For each helix, an initial analysis was performed on the last 5 ns of the trajectory in order to identify the average hinge point. Subsequent analyses on each helix were then performed with pre-specified hinge points, taken as the trajectory-averaged hinge residue. The hinge points for all of the helices, with the exception of M2 δ (chain C), lie near the centre of the pore in the vicinity of the hydrophobic residues α L251 (L9') and α V255 (L13') identified as the sites of the proposed hydrophobic gate by (Lester et al., 2004) and by Beckstein and Sansom (ms. in preparation) respectively. For M2 δ (chain C) the automatic location of the hinge point was complicated by the presence of δ P279 near the extracellular side of the helix bundle. For the purposes of comparison, however, we have examined the

distortion characteristics of this helix at the same predefined hinge point as those of the others. Having defined the hinge points, we analysed the kink and swivel angle conformational sampling of all five helices for the final 5 ns of the simulation. The polar plot (Fig. 4B) shows that the helices remain in a bent geometry throughout the simulation, but there are differences in the nature of the bending motion for each helix.

M2 α (A) exhibits the highest kink angle, varying between 15° to 45°, with an average of 30°. Helices M2 β (B), M2 α (D) and M2 γ (E) have somewhat lower kink angles, with averages of around 20°. Disregarding the proline-induced kink, chain M2 δ (C) exhibits the lowest bending, exceeding no more than 15° in general. Examination of the swivel angles reveals that helices M2 α (A), M2 β (B) and M2 γ (E) bend anisotropically, favouring a swivel angle range of around 60°. M2 α (D) samples a wider range of swivel angles (around 90°), while M2 δ (C) appears to bend isotropically, with no apparent preference for particular regions of swivel space. All of the helices exhibit swivel angle sampling in the same region of the polar plot. The anisotropic sampling of kink-swivel space may be understood by visual inspection of the structure, which reveals that all of the helices except M2 δ (C) bend towards the outer helices, with the C-terminal end towards M3 and the N-terminal end towards M1, while the apex of the kink points face towards the pore centre. Helix M2 δ (C) apparently remains nearly unkinked throughout the simulation, deviating little from its initial structure. Although the differences in the average kink/swivel conformations of the five helices in the current simulation might be expected to be due to differences in the primary structures of the subunits, it is interesting to note that MD simulations of homopentameric M2 δ bundles (Law et al., 2003) also revealed non-equal average kink angle distributions for each of the five helices. It is possible that, for both the current and previous simulations, such an asymmetry in helical conformations may be due to insufficient simulation time, and that on (for example) millisecond timescales the kink/swivel conformations for each helix may converge to a single

state. Possible implications of asymmetric motions are discussed below. Additionally, for the heteropentameric M2 bundle studied currently, differences in primary structure, especially in the M1 helix (see below), may well impart genuine differences on the M2 helical conformations and motions independent of timescale. In addition to structure, asymmetries also arise for the dynamical properties of each subunit M2, as discussed later.

We note that the region of helix kinking does not correspond to any known helix-distorting sequence motif. Thus, for the nAChR, there may be several external factors which influence the kink-swivel behaviour of the helices. Inspection of the motions of the M2s show that they shift closer towards the M1 and M3 helices in the early stages of the trajectory, possibly due to hydrophobic interactions between the M2s and the outer helices. However, for all subunits a relatively bulky hydrophobic sidechain near the centre of M1 (α F225 for chains α (A) and α (D), I for β 231(B), δ 239(C) and γ 233(E)) moves and points directly towards the M2 hinge point, and may therefore cause, or enhance, the degree of M2 helix bending due to steric repulsion. It is noteworthy that reverse mutagenesis studies of the M1 F and I residues (in which the F and I residues were swapped between the subunits) (Spitzmaul et al., 2004) revealed alterations in channel gating kinetics, but had no impact on ligand binding kinetics. Thus, given that the current simulation suggests a role for their sidechains in causing M2 helical bending, it is possible that the extent and nature of M2 helix bending may have an impact on gating kinetics, although the mechanistic rationale for this requires further study. Additionally, for chains α (A) and α (D), there are persistent hydrogen bonds between the hydroxyl group of the α S249 (M2, S6') sidechain and the backbone carbonyl of α L235 (M1) near the intracellular side, which may further help stabilise the M2 in a specific bent geometry. Finally, the motion of the M2-M3 loop is correlated with the degree of helix kinking (see below). Overall, then, there are forces driving the M2s towards the outer helices at the helix ends, and steric repulsion driving them towards the pore near the

centre. These combined forces create a tension which enhances the M2 bending angles from their initial values. For chain C, however, the tension is alleviated by pronounced bending at the proline residue near the extracellular side, preventing any more significant bending near the hydrophobic gate region. The current simulation therefore suggests an important role for the outer helix M1, and especially of the two residues discussed above, in imparting specific, anisotropic bending conformations upon the M2s, which may in turn influence their role in possible gating mechanisms.

Water and H-Bonding to the M2 Helices

In addition to hydrophobic interactions and specific residue-to-residue contacts with the M1 and M3 helices, the kinked conformations of M2 may also be stabilised by water-to-helix hydrogen bonding interactions at or near the hinge point which compete with intrahelical H-bonds. In order to determine the existence of such hinge-stabilising H-bonds between water and the protein backbone, we have estimated the water-to-backbone H-bond persistence ratio (R_H) for the final 5 ns of the simulation for each residue of all five M2 helices in the vicinity of the hinge point. The persistence ratio is defined as:

$$R_H = \frac{N_{AVERAGE}}{N_{TOTAL}}$$

where $N_{AVERAGE}$ is the average number of water-backbone H-bonds per timestep and N_{TOTAL} is the total number of *unique* H-bonds during this period. Thus, R_H may be regarded as proportional to the average time each unique H-bond is maintained during the trajectory segment; a “perfectly persistent” H-bond has $R_H = 1$. If the backbone traces of the M2 helices are colour-coded according to ranges of R_H values (Fig. 5) then persistence ‘hotspots’ are evident. For chain M2 α (A), two H-bond persistence ‘hotspots’ were identified, at α L251 (L9') and α V259 (V13'). These are both pore-facing residues approximately one helical turn on either side of the hinge point. The profile for chain M2 β (B) shows H-bond longevity at

β F262, also approximately one helix turn displaced from the hinge point. As previously discussed, chain M2 δ (C) exhibits the lowest average degree of helix bending if the hinge point is defined to lie near the pore centre. The comparatively low H-bond longevity is consistent with the small relative lack of helix distortion in this region. However, significant distortion near the extracellular end due to a Pro results in exposure of the backbone carbonyl to the pore waters, exhibiting a hotspot near this region. For chain M2 α (D), a single hotspot is located at α L258 (L16'), roughly one turn of the helix after the hinge point. Chain M2 γ (E) exhibits high H-bond persistence at γ L260 (L9') and γ A261 (A10'), i.e. one turn of the helix before the hinge point in the M2 sequence. Taken together, these results suggest that there are somewhat stronger, more long-lived H-bonds between water and the M2 backbones often one helical turn before the actual hinge point. Pore waters were found to form transient H-bonds mainly to backbone carbonyl O, with the highest H-bond persistence located at residues most exposed to the solvent environment due to deviations from helix linearity, and which are therefore most susceptible to competitive H-bonding from water. This suggest that water-backbone H-bonds may play a role in stabilising the kinked conformation of the M2 helices (as has been seen in water soluble proteins (Barlow and Thornton, 1988)), although other factors are likely have a greater influence on the conformation of the M2s.

Pore Profile and Cation Permeation Energetics

The possible influence of the M2 helix kinking on the function of the channel may be analysed in terms of pore radius profiles. The structures of the α M2s at 10 ns are shown in Fig. 6A, alongside a diagram of the pore-lining surface, and it may be seen that the hinge points lie adjacent to the major constriction in the centre of the pore (at α V255, i.e. V13'). The radius profiles of the channel at equidistant points along its axis for both the initial cryo-EM structure and averaged over the final 5ns of the MD simulation (dashed line) are compared in Fig. 6B. For the cryoEM structure, two constriction points are situated at α S248

(S6') and α L251 (L9'), with a third constriction located at α V255 (V13'). The constrictions at α L251 and α V255 corresponding to the proposed hydrophobic gate, and free energy profile calculations for a Na^+ ion within the M2 pore (Beckstein & Sansom, ms. in preparation) indicate a significant energy barrier ($\sim 8kT$) in this region. For the simulated structure, the constriction at α S248 is lost, being replaced by two constriction points at α L251 and α V255, with the latter showing the lowest average pore radius (~ 0.26 nm). However, as seen in Fig. 6B, the pore dimensions at these points fluctuate between ± 0.05 nm, so that at certain times during the trajectory it is possible for the relative radii of the two constriction points to be equal or even reversed. Thus, the pore radius calculations identify two regions of possible channel gating during the trajectory. The presence of multiple constriction regions may be responsible for possible ambiguities in identifying a unique residue of each subunit which form the channel gate.

Although quantification of the physical dimensions of the channel provides a qualitative insight into its permeability to ions, such an analysis by itself neglects the electrostatic contributions to this process. The polarity of pore-lining atoms is an important factor in ion conduction for acetylcholine receptors, since the hydrophobic girdle near the center of the channel is proposed to act as an energetic barrier to ions by means of water exclusion (Beckstein et al., 2001; Beckstein and Sansom, 2003; Beckstein and Sansom, 2004). Thus, in order to obtain a preliminary quantification of the energetics of trying to move a cation through the (closed) *Torpedo* nAChR channel we have computed the free energy of solvation (ΔG_{solv} , or Born energy) of a Na^+ ion at predefined positions along the pore axis. This calculation was performed within the framework of the continuum electrostatics model described by the Poisson-Boltzmann equation and implemented in the APBS code (Baker et al., 2001).

Born energy profiles were compared for four structures: the experimental EM structure (after energy minimisation), as well as three structures acquired from the final 5ns of the MD trajectory. The latter were chosen on the basis of constriction point radius, $R_{CONSTRUCT}$, i.e. the pore radius in the vicinity of the α V255 (V13') constriction. Three structures were selected, with $R_{CONSTRUCT} = 0.26$ nm, 0.19 nm and 0.29 nm. These structures had $R_{CONSTRUCT}$ values close to, below, and above the mean for the simulation respectively.

All of the Born energy profiles (Fig. 7) exhibit significant (i.e. $\gg kT$) peaks in the region of the α L251 (9') and α V255 (13') rings, effectively constituting energetic barriers to cation permeation, and providing confirmation that the initial experimental as well as MD snapshot structures describe the channel in a closed state. Comparison of the Born energy profiles with the corresponding pore radius profiles (not shown) show a close correspondence between Born energy barriers and pore constrictions (as might be anticipated). For the structure whose pore profile approximates that of the trajectory-average (i.e. the $R_{CONSTRUCT} = 0.26$ nm snapshot), the permeation barrier height is $\sim 15 kT$, comparable to that of the experimental structure with $\sim 18 kT$. For the $R_{CONSTRUCT} = 0.19$ nm structure the barrier height is $\sim 28 kT$. This suggests that although on average, the permeation barrier during an MD simulation is not significantly different from that of the EM structure, the barrier may fluctuate significantly. At the positions of the pore lined by the hydrophobic sidechains of residues α L251 (9') and α V255 (13'), the cation solvation energy increases with decreasing pore radius. These observations are consistent with the expectation that narrower regions of the pore, if lined by apolar sidechains, present a more hydrophobic environment in the neighbourhood of the cation, increasing the energetic cost of placing it there. Thus this analysis illustrates the principle of hydrophobic gating adopted by this and other ion channels (Beckstein et al., 2001; Beckstein and Sansom, 2004).

While for hydrophobic regions it is generally expected that the Born energy increases with respect to the narrowness of the confinement, the relationship between pore width and cation solvation energy may be more complex for regions of the channel lined by hydrophilic or charged residues. In all of the Born profiles presented here, an energy well exists at position α E262 (20'), likely due to the stabilisation of the Na^+ by the ring of negatively charged sidechains contributed from the α and β subunits. This stabilisation is more significant for the initial experimental structure, which has a well depth of $-5\text{ }kT$, and is less so for the MD derived structures, with well depths of roughly -1 to $-2\text{ }kT$. We note that the pore radii at the 20' position for the MD structures are all greater than the experimental structure, thus placing the sidechains further away from the Na^+ pathway and reducing the favourable cation-anion interactions. Although in the present work the electrostatic contributions from the ligand-binding domain are absent, it has been shown that for the $\alpha 7$ nAChR receptor the stabilisation described above for the *Torpedo* nAChR appears to be present as suggested by an energy well at 20', although the presence of the large extracellular (ligand binding) domain introduces a plateau of negative Born energy on the extracellular side above this position (Amiri et al., 2005).

The results discussed above therefore reveal that there are three points along the channel that may influence ion permeation; the L and V residues at the hydrophobic gate region forming an energetic barrier, and (perhaps less importantly) the negatively charged region forming a somewhat favourable electrostatic environment for cations. This suggests specific requirements for conformational changes that must occur during channel opening that will favour cation permeation, namely, enhancement of the pore width at 9' and 13' (and/or else rotation of the M2 helices so that more polar backbone atoms line the pore), and reduction in the pore width at 20' to optimise possible Na^+ -sidechain interactions. Helical-bending motions of the M2 helices is one possible way by which the above may be achieved;

a lesser bending angle may increase the pore radius near the hydrophobic centre, and simultaneously reduce the width at the charged 20' position. It is interesting therefore to note that helix bending is one of the concerted motions identified during the MD simulation (see discussion on principal components analysis below).

We note that the influence of atomic-level interactions between the cation, water and pore atoms, as well as entropic effects, have been neglected in the current model, averaged out by a continuum representation. These will certainly have an impact on the value of the solvation energy, especially for relatively narrow, hydrophobic regions of a pore. Atomic-level free energy calculations (such as umbrella sampling methods) are needed in order to obtain more quantitative results. We have performed investigations of the relationship between continuum models and atomic level free energy calculations for simple models of channels (Beckstein et al., 2004), the results of which suggest that continuum models may be adequate for illuminating the trends in the Born energy as a function of pore width and polarity.

Principal Components Analysis

We have investigated the possibility of concerted motions within the individual M2 helices using principal components analysis (or essential dynamics; (Amadei et al., 1993), enabling the visualisation of the directions and extents of the principal motions of C α atoms within the protein which move in a correlated fashion for a particular eigenvector projected along the trajectory. The first three eigenvectors account for roughly 45% of the motion observed in the last 5ns of the simulation trajectory, with cosine contents (Hess, 2000) of 8%, 39% and 3% respectively. These eigenvectors for the M2 α (A) helix (along with its attached M1-M2 and M2-M3 loops) are shown in Fig. 8A-C. All three eigenvectors indicate concerted motions between the extramembranous loops (and the M2-M3 loop in particular) with movements of the helical region atoms. However, the particular helical motions differ

between the eigenvectors. The first eigenvector (EV1) shows unidirectional motion of the helical segments, all of which move towards the direction of the outer helices, with some bias towards the extracellular side, corresponding to collapse of M2 against the rigid scaffold. EV2 exhibits intra-helical movements, with downwards motions for the upper half of the helix, and upwards motions for the lower half, resembling a helix bending motion, as identified by SWINK analysis (discussed above). Finally, EV3 suggests rotational motion of the entire helix. Similar analyses for the other M2 helices reveal qualitatively similar results (not shown). In sum, the first three EVs indicate that the motions of the M2-M3 linker loop are highly correlated with bending, translational and rotational motions of the M2 helix relative to the scaffold helices. Since the mechanism of gating is currently proposed to involve such motions, this analysis reinforces the notion that conformational changes at the LBD may be transmitted to the pore via the M2-M3 linker, and furthermore suggests that helix bending may also play a role in gating. In particular, helix bending motions may play an important role in channel gating by altering the height of the permeation energy barrier at the hydrophobic girdle as well as the depth of the energy well near the extracellular end of the TM domain, thus mediating the degree of interaction between cations and the pore.

PCA was also performed on the entire five M2 helix bundle, excluding the extramembranous loops in order to elucidate the more subtle motions between the helical regions, discarding the rather large correlated motions of the more flexible regions. The resultant first eigenvector (cosine content of 23%) is shown in Fig. 8D. As with the PCA of the individual subunits, several motions may be identified. The two α subunits and the γ subunit appear to rotate in the same sense. The β M2 also undergoes some degree of rotation, to a lesser extent. The δ subunit, however, mainly undergoes to-and-fro translational motions relative to the outer helices. The helices therefore rotate asymmetrically, as might be expected from the heteropentameric nature of the bundle. Dynamical asymmetry has also

been observed in simulations of a homology model of the homopentameric $\alpha 7$ LBD (Henchman et al., 2003), and in simulations of the intracellular ligand-binding domain of inward rectifier (Kir) channels (Haider et al., 2004). These results suggest that asymmetric motions may be inherent in multimeric ion channels regardless of subunit composition. If so, this might suggest that a fully concerted model of conformational change (Galzi and Changeux, 1994) may not apply to ion channel gating, and that instead sequential propagation of conformational change through the constituent subunits (Grosman et al., 2000; Cymes et al., 2002) may be a more appropriate model, as suggested by *inter alia* (Lester et al., 2004).

The rotational motion apparent in EV1 is reminiscent of the rotation of the M2 helices in the proposed gating model; inspection of the positions of the constriction point V sidechains between the two extreme projections of EV1 shows their motion away from the centre of the pore, and HOLE calculations of the pore radius shows a change of around 0.2 Å between the two structures. However, caution should be exercised in interpreting the results of the PCA. The short timescale of the current simulation is such that an actual and complete channel opening event is unlikely to be observed. Indeed, the pore profile calculation shows that, although there is some fluctuation of the minimum pore radius during the trajectory, the channel is essentially in a closed state throughout. Thus, the PCA results are simply indicative of the intrinsic flexibility of the gate region of the TM domain. Nonetheless, it is in principle feasible that, without the presence of the ligand binding domain to hold the M2-M3 loops in place, there would be greater freedom for the M2 helices to fluctuate between closed and open states, and thus it is possible that even on a 10ns timescale motions which are important for channel gating may be observed.

Normal Mode Analysis of a Coarse-Grained Model

A limitation of the preceding analysis is the relatively short timescale (10 ns) of atomistic MD simulations compared to that of gating transitions within the (intact) nAChR. We have attempted to estimate the extent to which the atomistic simulations are able to describe low frequency collective motions (which may be relevant to our understanding of channel gating) by using a more coarse-grained model of the protein motions. Accordingly, we have applied NMA within an ANM to identify possible global modes for the motions of both the initial (i.e. from cryo-EM) and final MD (i.e. $t = 10$ ns) TM structures in order to obtain qualitative insights into their collective motions as well as to serve as a comparison with results of PCA analysis of the MD simulations discussed above.

Although the use of a coarse-grained model with an uniform inter-residue interaction parameter results in the loss of detailed information about smaller scale, local fluctuations (which are usually sidechain specific), it has been shown (Bahar et al., 1997; Atilgan et al., 2001) that slow, large-scale collective motions are mainly dependent on the tertiary structure of the protein, and may be adequately described by a simple network model.

Despite these advantages it is unclear whether, in general, NMA-based methods are entirely suitable for studying motions related to the function of ligand-gated ion channels. There are likely to be significant energy barriers separating the closed and opened states due to mechanical constraints imposed by the extracellular domain, resulting in anharmonicity of the energy surface. However, in the present case, such energy barriers are missing due to the exclusion of the LBD in the model. The energy surface may therefore be anticipated to exhibit a lower degree of anharmonicity compared to that of the full length receptor, and hence motions in the TM domain which contribute to channel function are more likely to be amenable to study by NMA methods. Obviously, barriers to gating are still likely to exist owing to internal interactions within the TM domain, and an actual channel opening motion

may not be revealed by NMA. Nevertheless, previous studies on ion channels such as MscL (Valadie et al., 2003) and KcsA (Shen et al., 2002) have shown that NMA is capable of revealing motions relevant for gating despite the lack of channel opening motions. In the present work, therefore, the key assumption is that the collective motions of the regions with the lowest deformation energies, in the absence of the LBD mechanical constraints, are relevant for biological function.

We note that for the MD simulation, the M1 and M3 helices were restrained. However for the ANM model no such restraints were applied. Thus the results obtained from NMA are unlikely to correspond exactly with those from the MD, in that the NMA will reveal motions of the outer helices. However, the motions of the M2 helices (as with all parts of the protein) are governed entirely by their connectivities to other regions, namely the M1 and M3 helices, as well as neighbouring subunits. These are constant, and are exactly the same whether the outer helices are motionally restrained or not. Thus the character of the motions of the M2 helices relative to a fixed point (eg. the pore centre) should not differ significantly. For the purposes of comparison with the MD/PCA results, we focus exclusively on the motions of the “free” components (i.e. the M2-M3 loops, the M2 helices and M2-M1 loops).

The lowest frequency normal modes of both the initial structure and an MD-acquired 10 ns structure were investigated. We note that for the MD structure, those obtained from several other timeframes within the last 5ns of the trajectory showed similar results (not shown). As usual, the first 6 modes correspond to eigenvectors with zero eigenvalues (i.e. translations and rotations) and are discarded; the lowest frequency normal mode is mode 7. For the 1OED structure, mode 7 (see Fig. 9A) describes mainly translational fluctuations of the M2-M3 loops, together with the upper part of the M2 helices, with respect to the pore center. This is asymmetric in terms of the pentameric bundle, with the α M2's motions directly opposite of those of the γ and δ subunits. The β M2's move along a line roughly

tangential with respect to the pore. Qualitatively similar motions are identified for the 10ns MD structure (not shown), however, here chain $\alpha(A)$ moves in an opposite direction to those of $\beta(B)$ and $\gamma(E)$, while $\delta(C)$ and $\alpha(D)$ show translation tangential to the pore. The nature of the translational motions results in a bending motion for all of the M2 helices, with the hinge point located approximately at the helix centre (i.e. near $\alpha V255$ (see Fig. 9B & C). This highlights the possibility that the intrinsic flexibility of the M2's can also arise from the nature of the protein topology; there is lower flexibility at the bottom half of the M2's due to greater connectivities with neighbouring subunits, while the opposite is true for the upper half. Coupled with the freedom of the M2-M3 loops, the extracellular half may therefore undergo greater motions, resulting in helix bending even without hinge-bending motifs (e.g. involving Gly or Pro) near the kink point. Similar motions are described by mode 8 for 1OED, and modes 8, 9 and 10 for the 10 ns MD snapshot. Other normal modes also exhibit motions which resemble those identified by PCA. Mode 9 for the cryo-EM structure suggests symmetric and unidirectional rotation of the M2 helices, while asymmetric rotations (involving only three out of five M2 helices) were observed for the MD structure in modes 11 and 12. However, these rotations do not result in significant pore widening. We note that higher frequency modes for both structures reveal relatively localised fluctuations, such as those restricted to single M2-M3 loops and helix ends, and are not considered here

Although the agreement between the timescale-independent ANM/NMA and the timescale-dependent MD/PCA is not exact, the characteristics of the collective motions identified using the two approaches show some consistency, and are indicative of the robustness of different methodological approaches to the results. This has several possible interpretations. At the single-helix level, the similarity of the motions (namely, translational, rotational and bending motions of the M2 helices correlated with motions of the M2-M3 loops) identified with the different methods simply illustrates that there are only a limited

number of collective motions possible for the helices, given their structural arrangement, and that the directions of these motions are relatively insensitive to timescale beyond several ns. At the 5-helix bundle level, PCA analysis of the MD trajectory extracted (in the 1st eigenvector) partial concerted rotations of the M2 helices, similar in nature to those extracted from NMA (in mode 9 for 1OED and modes 11 and 12 for the MD) of the ANM results, showing that the MD trajectory has partially described some of the major collective motions identified by ANM. This suggests that the energy landscape within the conformational space sampled during the MD run (i.e. for the closed state only) is approximately harmonic. However, further exploration (e.g. by lengthier simulations) of the conformational space of the nAChR is required in order to determine the validity of this approximation for regions of the energy surface further from those visited in the current trajectory. It is of some interest to consider the timescale that such, inevitably coarse-grained, simulations will have to address. Recent kinetic studies suggest a timescale of $\sim 1 \mu\text{s}$ for the channel opening conformational transition (Chakrapani and Auerbach, 2005). Given recent progress in achieving such times for atomistic simulations of peptide folding (Duan and Kollman, 1998; Simmerling et al., 2002) it is reasonable to assume that appropriately coarse-grained channel simulations should be able to achieve such a timescale in the near future.

CONCLUSIONS

In this study we have used MD simulation to explore possible changes in conformation of the M2 helix bundle of the nAChR, starting from the 1OED structure built on the basis of 4 Å resolution EM images of the transmembrane domain. These conformational changes are presumed to reflect two factors: ‘relaxation’ of a model based upon medium resolution data, and intrinsic flexibility of the inner M2 helix bundle within the (restrained) outer bundle formed by the M1, M3 and M4 helices. Analysis of the simulation

data reveals two key aspects of the behaviour of the M2 helices: a M2 helix kinking motion, and asymmetry in the conformational dynamics of the M2 helix bundle. The kinking of the M2 helices leads to a narrowing of the pore in the vicinity of the proposed hydrophobic gate (residues L9' and V13' of M2). The asymmetry of the M2 helix motions is suggestive of a sequential rather than a concerted model of channel gating, although a concerted model with asymmetric motions cannot be excluded.

How are these simulation results related to experimental studies of nAChR and related members of the Cys-loop receptor channel family? The kinking of the helices to constrict the pore in the vicinity of the L9' and V13' hydrophobic rings is consistent with a body of data that places the gate in this vicinity (summarised in e.g. (Lester, 1992; Lester et al., 2004; Bertrand et al., 1993; Corringer et al., 2000), also (Panicker et al., 2002)). The majority of the nAChR data have been interpreted in terms of a gate at L9', although it may be difficult to be precise to within one turn of the M2 helix in positioning a gate by mutagenesis and labelling studies. The asymmetry of the M2 helix conformational dynamics would seem to be broadly consistent with the 'conformational wave' model of nAChR gating (Grosman et al., 2000; Cymes et al., 2002; Mitra et al., 2004), although as discussed above, caution must be exercised in interpreting the implications of the dynamics exhibited in the current simulations due to the discordant timescales of MD simulations and channel gating in reality. We have therefore correlated the results of our (short timescale) atomistic simulations with the outcome of more coarse-grained simulations using a Gaussian network model.

It is useful to place these results in the context of related theoretical and simulation studies of nAChR. There have been a number of modelling (Sankararamakrishnan and Sansom, 1995; Kim et al., 2004) and simulation studies of pores formed by *just* the M2 helix bundle (Law et al., 2003; Saiz and Klein, 2002; Saiz et al., 2004), inspired by structural and functional data on channels formed by an M2 helix peptide (Oiki et al., 1988; Montal et al.,

1993; Montal, 1995; Opella et al., 1999). However, the EM structure, despite the limitations of resolution, indicates that the packing of the M2 helices is modified by the presence of the outer (M1,M3,M4) helix bundle. The structure of the intact TM domain supports the model of a hydrophobic gate in the centre of the M2 helix bundle. The feasibility of such a hydrophobic gating model is supported by MD simulations of water (Beckstein et al., 2001; Beckstein and Sansom, 2003) and of ions (Beckstein and Sansom, 2004) in simplified models of ion channels, and by simulations of the putative hydrophobic gate of the MscS mechanosensitive channel (Anishkin and Sukharev, 2004). Recent continuum electrostatics calculations (Corry, 2004) also support such a gating model for the nAChR, although the results of such calculations should be treated with some caution in the light of comparisons of continuum electrostatics and atomistic PMF calculations of barriers to ion permeation in simple model pores (Beckstein et al., 2004). Thus, the results of the current simulations are consistent with and extend the emergent theoretical model of hydrophobic gating in the nAChR.

The indications of asymmetric conformational dynamics in the M2 helix bundle are significant, especially as comparable asymmetries have been observed in MD simulations of the extracellular ligand-binding domain of the homopentameric $\alpha 7$ nAChR (Henchman et al., 2003). Furthermore, recent kinetic analysis of mutants in the M4 helices of the nAChR (Mitra et al., 2004) have been interpreted in terms of movement of the α subunits before the ϵ and β subunits (in mouse nAChR the ϵ subunit replaces the γ subunit of the nAChR). Of course, the timescale of the current MD simulations (10 ns) falls several orders of magnitude short of the timescale of channel activation in response to acetylcholine binding (~ 1 ms). However, it may be that the short timescale intrinsic flexibility of the M2 helices reveals at least some aspects of the dynamics of the *gate* which are modulated within the intact receptor-channel protein by coupling to the wave of conformational change propagated down the protein

(Grosman et al., 2000; Cymes et al., 2002) following binding of the agonist to the receptor (i.e. *gatekeeper*) domain. It is of interest that M2 bending is seen in the coarse-grained calculations, suggesting that in part this may reflect the environment which the remainder of the TM domain presents to these helices.

It is important to consider two limitations of the current simulation study. One is the absence of the ligand-binding domain and intracellular vestibule from the model, necessitating the use of restraints to maintain the integrity of the outer (M1,M3,M4) helix bundle. The other is the use of an octane slab to approximate the membrane environment, rather than a lipid bilayer. In particular, the lipid bilayer headgroups will influence water ordering at the membrane/water interface.

To address this we have recently completed unrestrained MD simulations of the TM domain in a lipid bilayer (Hung and Sansom, manuscript in preparation) which yield several results that are in qualitative agreement with those discussed in the current manuscript. In particular, these latter studies indicate, that the minimum pore radius is significantly reduced compared to that of the initial EM structure, and that several M2 helices exhibit a significantly kinked conformation with the hinge point residues coinciding with those described in the current manuscript. We are therefore reasonably confident that the behaviour of M2 described above is unlikely to be a simulation artefact due to the use position restraints. However, more detailed analysis and comparison of theses and of other recent simulations (Xu et al., 2005) will be needed to clear as to the possible influence of protein/lipid interactions.

Acknowledgements

Our thanks to Nigel Unwin for his valuable discussions on the structure of the receptor, Oliver Beckstein for his help in performing pK_a and Born energy profile calculations, and

Phil Biggin and Shiva Amiri for their advice on the current work. We also thank the EPSRC, BBSRC, and Wellcome Trust for financial support, and finally all of our colleagues for their advice and encouragement.

REFERENCES

- Adcock, C., G. R. Smith, and M. S. P. Sansom. 1998. Electrostatics and the ion selectivity of ligand-gated ion channels. *Biophys. J.* 75:1211-1222.
- Adcock, C., G. R. Smith, and M. S. P. Sansom. 2000. The nicotinic acetylcholine receptor: from molecular model to single channel conductance. *Eur. Biophys. J.* 29:29-37.
- Amadei, A., A. B. M. Linssen, and H. J. C. Berendsen. 1993. Essential dynamics of proteins. *Proteins: Struc. Func. Genet.* 17:412-425.
- Amiri, S., K. Tai, O. Beckstein, P. C. Biggin, and M. S. P. Sansom. 2005. The $\alpha 7$ nicotinic acetylcholine receptor: molecular modelling, electrostatics, and energetics. *Mol. Memb. Biol.* (in press).
- Anishkin, A., and S. Sukharev. 2004. Water dynamics and dewetting transitions in the small mechanosensitive channel MscS. *Biophys. J.* 86:2883-2895.
- Atilgan, A. R., S. R. Durell, R. L. Jernigan, M. C. Demirel, O. Keskin, and I. Bahar. 2001. Anisotropy of fluctuation dynamics of proteins with an elastic network model. *Biophys. J.* 80:505-515.
- Bahar, I., A. R. Atilgan, and B. Erman. 1997. Direct evaluation of thermal fluctuations in proteins using a single-parameter harmonic potential. *Fold. Des.* 2:173-181.
- Baker, N. A., D. Sept, S. Joseph, M. J. Holst, and J. A. McCammon. 2001. Electrostatics of nanosystems: application to microtubules and the ribosome. *Proc. Nat. Acad. Sci. USA.* 98:10037-10041.
- Barlow, D. J., and J. M. Thornton. 1988. Helix geometry in proteins. *J. Mol. Biol.* 201:601-619.
- Barrett, C. P., B. A. Hall, and M. E. M. Noble. 2004. Dynamite: a simple way to gain insight into protein motions. *Acta Cryst. D.* 60:2280-2287.

- Beckstein, O., P. C. Biggin, P. J. Bond, J. N. Bright, C. Domene, A. Grottesi, J. Holyoake, and M. S. P. Sansom. 2003. Ion channel gating: insights via molecular simulations. *FEBS Lett.* 555:85-90.
- Beckstein, O., P. C. Biggin, and M. S. P. Sansom. 2001. A hydrophobic gating mechanism for nanopores. *J. Phys. Chem. B.* 105:12902-12905.
- Beckstein, O., and M. S. P. Sansom. 2003. Liquid–vapor oscillations of water in hydrophobic nanopores. *Proc. Nat. Acad. Sci. USA.* 100:7063-7068.
- Beckstein, O., and M. S. P. Sansom. 2004. The influence of geometry, surface character and flexibility on the permeation of ions and water through biological pores. *Phys. Biol.* 1:42-52.
- Beckstein, O., K. Tai, and M. S. P. Sansom. 2004. Not ions alone: barriers to ion permeation in nanopores and channels. *J. Amer. Chem. Soc.* 126:14694-14695.
- Berendsen, H. J. C., J. P. M. Postma, W. F. van Gunsteren, A. DiNola, and J. R. Haak. 1984. Molecular dynamics with coupling to an external bath. *J. Chem. Phys.* 81:3684-3690.
- Berendsen, H. J. C., J. P. M. Postma, W. F. van Gunsteren, and J. Hermans. 1981. Intermolecular Forces. Reidel, Dordrecht.
- Bertrand, D., J. L. Galzi, A. Devillers-Thiéry, S. Bertrand, and J. P. Changeux. 1993. Stratification of the channel domain in neurotransmitter receptors. *Curr. Opin. Cell Biol.* 5:688-693.
- Bright, J. N., I. H. Shrivastava, F. S. Cordes, and M. S. P. Sansom. 2002. Conformational dynamics of helix S6 from Shaker potassium channel: simulation studies. *Biopolymers.* 64:303-313.
- Chakrapani, S., and A. Auerbach. 2005. A speed limit for conformational change of an allosteric membrane protein. *Proc. Natl. Acad. Sci. USA.* 102:87-92.

- Changeux, J. P., J. I. Galzi, A. Devillers-Thiéry, and D. Bertrand. 1992. The functional architecture of the acetylcholine nicotinic receptor explored by affinity labelling and site-directed mutagenesis. *Quart. Rev. Biophys.* 25:395-432.
- Cordes, F. S., J. N. Bright, and M. S. P. Sansom. 2002. Proline-induced distortions of transmembrane helices. *J. Mol. Biol.* 323:951-960.
- Cornell, W. D., P. Cieplak, C. I. Bayly, I. R. Gould, K. M. Merz, D. M. Ferguson, D. C. Spellmeyer, T. Fox, J. W. Caldwell, and P. A. Kollman. 1995. A second generation force field for the simulation of proteins and nucleic acids. *J. Am. Chem. Soc.* 117:5179-5197.
- Corringer, P. J., N. Le Novere, and J. P. Changeux. 2000. Nicotinic receptors at the amino acid level. *Ann. Rev. Pharmacol. Toxicol.* 40:431-458.
- Corry, B. 2004. Theoretical conformation of the closed and open states of the acetylcholine receptor channel. *Biochim. Biophys. Acta.* 1663:2-5.
- Cymes, G. D., C. Grosman, and A. Auerbach. 2002. Structure of the transition state of gating in the acetylcholine receptor channel pore: A F-value analysis. *Biochem.* 41:5548-5555.
- Darden, T., D. York, and L. Pedersen. 1993. Particle mesh Ewald - an N.log(N) method for Ewald sums in large systems. *J. Chem. Phys.* 98:10089-10092.
- Dolinsky, T. J., J. E. Nielsen, J. A. McCammon, and N. A. Baker. 2004. PDB2PQR: an automated pipeline for the setup, execution, and analysis of Poisson-Boltzmann electrostatics calculations. *Nucl. Acids Res.* 32:W665-667.
- Duan, Y., and P. A. Kollman. 1998. Pathway to a folding intermediate observed in a microsecond simulation in aqueous solution. *Science.* 282:740-744.
- Essmann, U., L. Perera, M. L. Berkowitz, T. Darden, H. Lee, and L. G. Pedersen. 1995. A smooth particle mesh Ewald method. *J. Chem. Phys.* 103:8577-8593.

- Faraldo-Gómez, J. D., L. R. Forrest, M. Baaden, P. J. Bond, C. Domene, G. Patargias, J. Cuthbertson, and M. S. P. Sansom. 2004. Conformational sampling and dynamics of membrane proteins from 10-nanosecond computer simulations. *Proteins: Struct. Func. Bioinf.* (in press).
- Faraldo-Gómez, J. D., G. R. Smith, and M. S. P. Sansom. 2003. Molecular dynamics simulations of the bacterial outer membrane protein FhuA: a comparative study of the ferrichrome-free and bound states. *Biophys. J.* 85:1-15.
- Galzi, J. L., and J. P. Changeux. 1994. Neurotransmitter-gated ion channels as unconventional allosteric proteins. *Curr. Opin. Struct. Biol.* 4:554-565.
- Grosman, C., M. Zhou, and A. Auerbach. 2000. Mapping the conformational wave of acetylcholine receptor channel gating. *Nature.* 403:773-776.
- Haider, S., A. Grottesi, F. M. Ashcroft, and M. S. P. Sansom. 2004. Conformational dynamics of the ligand-binding domain of inward rectifier K channels as revealed by MD simulations: towards an understanding of Kir channel gating. *Biophys. J.* (submitted).
- Henchman, R. H., H. L. Wang, S. M. Sine, P. Taylor, and J. A. McCammon. 2003. Asymmetric structural motions of the homomeric $\alpha 7$ nicotinic receptor ligand binding domain revealed by molecular dynamics simulation. *Biophys. J.* 85:3007-3018.
- Hess, B. 2000. Similarities between principal components of protein dynamics and random diffusion. *Phys. Rev. E.* 62:8438-8448.
- Hess, B., H. Bekker, H. J. C. Berendsen, and J. G. E. M. Fraaije. 1997. LINCS: A linear constraint solver for molecular simulations. *J. Comp. Chem.* 18:1463-1472.
- Hille, B. 2001. Ionic Channels of Excitable Membranes. Sinauer Associates Inc., Sunderland, Mass.

- Humphrey, W., A. Dalke, and K. Schulten. 1996. VMD - Visual Molecular Dynamics. *J. Molec. Graph.* 14:33-38.
- Kabsch, W., and C. Sander. 1983. Dictionary of protein secondary structure: pattern-recognition of hydrogen-bonded and geometrical features. *Biopolymers.* 22:2577-2637.
- Karlin, A. 2002. Emerging structure of the nicotinic acetylcholine receptors. *Nature Rev. Neurosci.* 3:102-114.
- Karlin, A., and M. H. Akabas. 1995. Toward a structural basis for the function of nicotinic acetylcholine receptors and their cousins. *Neuron.* 15:1231-1244.
- Kim, S., A. K. Chamberlain, and J. U. Bowie. 2004. A model of the closed form of the nicotinic acetylcholine receptor M2 channel pore. *Biophys. J.* 87:792-799.
- Law, R. J., L. R. Forrest, K. M. Ranatunga, P. La Rocca, D. P. Tieleman, and M. S. P. Sansom. 2000. Structure and dynamics of the pore-lining helix of the nicotinic receptor: MD simulations in water, lipid bilayers and transbilayer bundles. *Proteins: Struct. Func. Genet.* 39:47-55.
- Law, R. J., D. P. Tieleman, and M. S. P. Sansom. 2003. Pores formed by the nicotinic receptor M2d peptide: a molecular dynamics simulation study. *Biophys. J.* 84:14-27.
- Lester, H. 1992. The permeation pathway of neurotransmitter-gated ion channels. *Ann. Rev. Biophys. Biomol. Struct.* 21:267-292.
- Lester, H. A., M. I. Dibas, D. S. Dahan, J. F. Leite, and D. A. Dougherty. 2004. Cys-loop receptors: new twists and turns. *Trends Neurosci.* 27:329-336.
- Lindahl, E., B. Hess, and D. van der Spoel. 2001. GROMACS 3.0: a package for molecular simulation and trajectory analysis. *J. Molec. Model.* 7:306-317.
- Lummis, S. C. R. 2004. The transmembrane domain of the 5-HT₃ receptor: its role in selectivity and gating. *Biochem. Soc. Trans.* 32:535-539.

- Mitra, A., T. D. Bailey, and A. Auerbach. 2004. Structural dynamics of the M4 transmembrane segment during acetylcholine receptor gating. *Structure*. 12:1909-1918.
- Miyazawa, A., Y. Fujiyoshi, and N. Unwin. 2003. Structure and gating mechanism of the acetylcholine receptor pore. *Nature*. 423:949-955.
- Montal, M. 1995. Design of molecular function: channels of communication. *Ann. Rev. Biophys. Biomol. Struct.* 24:31-57.
- Montal, M. O., T. Iwamoto, J. M. Tomich, and M. Montal. 1993. Design, synthesis and functional characterisation of a pentameric channel protein that mimics the presumed pore structure of the nicotinic cholinergic receptor. *FEBS Lett.* . 320:261-266.
- Oiki, S., W. Danho, V. Madison, and M. Montal. 1988. M2d, a candidate for the structure lining the ionic channel of the nicotinic cholinergic receptor. *Proc. Natl. Acad. Sci. USA*. 85:8703-8707.
- Opella, S. J., F. M. Marassi, J. J. Gesell, A. P. Valente, Y. Kim, M. Oblatt-Montal, and M. Montal. 1999. Structures of the M2 channel-lining segments from nicotinic acetylcholine and NMDA receptors by NMR spectroscopy. *Nature Struct. Biol.* 6:374-379.
- Panicker, S., H. Cruz, C. Arrabit, and P. A. Slesinger. 2002. Evidence for a centrally located gate in the pore of a serotonin-gated ion channel. *J. Neurosci.* 22:1629-1639.
- Rashin, A., and B. Honig. 1985. Reevaluation of the Born model of ion hydration. *J. Phys. Chem.* 89:5588.
- Saiz, L., S. Bandyopadhyay, and M. L. Klein. 2004. Effect of the pore region of a transmembrane ion channel on the physical properties of a simple membrane. *J. Phys. Chem. B*. 108:2608-2613.

- Saiz, L., and M. L. Klein. 2002. Computer simulation studies of model biological membranes. *Acc. Chem. Res.* 35:482-489.
- Sankararamakrishnan, R., C. Adcock, and M. S. P. Sansom. 1996. The pore domain of the nicotinic acetylcholine receptor:- molecular modelling and electrostatics. *Biophys. J.* 71:1659-1671.
- Sankararamakrishnan, R., and M. S. P. Sansom. 1995. Modelling packing interactions in parallel helix bundles:- pentameric bundles of nicotinic receptor M2 helices. *Biochim. Biophys. Acta.* 1239:122-132.
- Shen, Y. F., Y. F. Kong, and J. P. Ma. 2002. Intrinsic flexibility and gating mechanism of the potassium channel KcsA. *Proc. Nat. Acad. Sci. USA.* 99:1949-1953.
- Simmerling, C., B. Strockbine, and A. E. Roitberg. 2002. All-atom structure prediction and folding simulations of a stable protein. *J. Am. Chem. Soc.* 124:11258-11259.
- Smart, O. S., J. G. Neduvellil, X. Wang, B. A. Wallace, and M. S. P. Sansom. 1996. Hole: A program for the analysis of the pore dimensions of ion channel structural models. *J. Mol. Graph.* 14:354-360.
- Spitzmaul, G., J. Corradi, and C. Bouzat. 2004. Mechanistic contributions of residues in the M1 transmembrane domain of the nicotinic receptor to channel gating. *Mol. Memb. Biol.* 21:39-50.
- Tai, K., T. Shen, U. Börjesson, M. Philippopoulos, and J. A. McCammon. 2001. Analysis of a 10-ns molecular dynamics simulation of mouse acetylcholinesterase. *Biophys. J.* 81:715-724.
- Tai, K., T. Shen, R. H. Henchman, Y. Bourne, P. Marchot, and J. A. McCammon. 2002. Mechanism of acetylcholinesterase inhibition by fasciculin: a 5-ns molecular dynamics simulation. *J. Am. Chem. Soc.* 124:6153-6161.

- Tikhonov, D. B., and B. S. Zhorov. 1998. Kinked-helices model of the nicotinic acetylcholine receptor ion channel and its complexes with blockers: Simulation by the Monte Carlo minimization method. *Biophys. J.* 74:242-255.
- Unwin, N. 1993. Nicotinic acetylcholine receptor at 9 Å resolution. *J. Mol. Biol.* 229:1101-1124.
- Unwin, N. 1995. Acetylcholine receptor channel imaged in the open state. *Nature.* 373:37-43.
- Valadie, H., J. J. Lacapcre, Y. H. Sanejouand, and C. Etchebest. 2003. Dynamical properties of the MscL of Escherichia coli: A normal mode analysis. *J. Mol. Biol.* 332:657-674.
- van Gunsteren, W. F., P. Kruger, S. R. Billeter, A. E. Mark, A. A. Eising, W. R. P. Scott, P. H. Huneberger, and I. G. Tironi. 1996. Biomolecular Simulation: The GROMOS96 Manual and User Guide. Biomos & Hochschulverlag AG an der ETH Zurich, Groningen & Zurich.
- Vriend, G. 1990. WhatIf - a molecular modeling and drug design program. *J. Mol. Graph.* 8:52-56.
- Xu, Y., F. J. Barrantes, X. Luo, K. Chen, J. Shen, and H. Jiang. 2005. Conformational dynamics of the nicotinic acetylcholine receptor channel: a 35-ns molecular dynamics simulation study. *J. Am. Chem. Soc.* (in press).

FIGURES

Figure 1:

Sequences of the M2 helices as defined in the 1OED pdb file. The 9' residue (α L251) thought to lie at the gate (Lester et al., 2004) is in **bold** and the 13' residue (α V255) at the helix kink (this study) is underlined. The extents of the M2 helices are: α K242 - α V271, β K248 - β V277, δ K256 - δ V285, and γ Q250 - γ V280.

Figure 2:

A Structure of the nAChR transmembrane helices and loops viewed along the channel (z) axis from the extracellular mouth down towards the intracellular side. Greyed regions were positionally restrained during the MD simulations, while the coloured regions underwent unrestrained motions. Subunits are named as follows: A = α (red), B = β (blue), C = δ (yellow), D = α (red), and E = γ (green). **B** Structure viewed perpendicular to the bilayer normal, with the locations of the octane-water interface boundaries in the initial simulation setup indicated.

Figure 3:

A Root-mean-square deviation (RMSD) of the C α atoms of the five M2 helices from their initial conformations with respect to simulation time. RMSD curves for the individual M2 helices are coded as follows: thick black solid line = averaged over all subunits; black broken line = M2 α (A); grey dotted line = M2 β (B); grey solid line = M2 δ (C); black dotted line = chain M2 α (D); and grey broken line = M2 γ (E). **B** Root-mean-square fluctuation (RMSF) of the C α atoms of the five M2 helices and M2-M3 loops. Chain identifiers for the atoms are shown along the x-axis; for each chain, the N-terminus of the M2 helix is at the left, while the C-terminus of the M2-M3 loop is at the right. The residue numbers on the x-axis are as

follows: 1 - 29 = M2 and M2-M3 loop of subunits α (A); 30 - 58 = subunit β (B); 59 - 87 = subunit δ (C); 89 - 116 = subunit α (D); and 117 - 145 = subunit γ (E).

C Block analysis of mean square fluctuations (MSFs; calculated for Ca atoms). For the final 8 ns of each simulation, average MSF values were calculated for time windows of 0.1, 0.25, 0.5, 1, 2.5 and 5ns. MSF values were evaluated separately for the M1-M2 (solid grey line), M2-M3 loops (broken black line), and for the M2 helical regions (solid black line).

Figure 4:

A Ca trace diagrams of helix M2 α (chain A) from the cryo-EM structure (1oed) and from the simulation at 0, 0.5, 1, 5 and 10 ns. The approximate location of the hinge (residue α V255) is indicated by an arrow. **B** Polar plot representation of the kink and swivel angles sampled by the five M2 helices during the last 5 ns of simulation. Black = M2 α (A), red = M2 β (B), green = M2 δ (C), blue = chain M2 α (D), cyan = M2 γ (E). The kink angle is plotted in the radial axis and the swivel angle on the circumferential axis. The swivel angle is defined as the rotation of the post-hinge helix vector in the plane perpendicular to the pre-hinge vector relative to a zero point, set at the C α of the hinge residue, when viewed along the helix from the C terminal (see Cordes et al. (2002) for further details).

Figure 5:

Tube representations of the central segments of M2 helices α (A), β (B), δ (C), α (D) and γ (E), colour graded according to their water-to-backbone H-bond persistence (R_H ; see text for definition), ranging (on the RGB scale) from red = high R_H to blue = low R_H .

Figure 6:

A Simulation snapshot of the M2 and M1 backbone atoms of the two α subunits at 10 ns, with the pore-lining surface determined using HOLE (Smart et al., 1996), and constriction point close to α V255 indicated by an arrow. Black spheres near the M2 centres indicate the Ca atoms of kink points determined using SWINK (Cordes et al., 2002). Residues of interest are coloured in pale grey (see text). Other subunits have been omitted for clarity. **B** Pore radius profile as a function of position along the pore (z) axis. The thick black line shows the pore radius profile for the initial (1OED) structure, while the solid grey line indicates the mean pore radius profile (\pm standard deviation) averaged over the last 5 ns of simulation.

Figure 7:

Sodium ion (Na^+ , Born radius 1.69 Å) solvation free energy (Born energy) profiles for the experimental structure **A** (continuous black line), and for three snapshots from the latter half of the simulation for which $R_{\text{CONSTRUCT}} = 0.19$ nm (continuous grey line), 0.26 nm (broken black line), and 0.29 nm (broken grey line), where $R_{\text{CONSTRUCT}}$ is the pore radius in the vicinity of the α V255 (V13') constriction.

Figure 8:

A-C Porcupine plots (Tai et al., 2001; Tai et al., 2002) of the first 3 eigenvectors describing the motion of the M2 helix plus loops from chain A. **D** Porcupine plot of the M2 helix bundle.

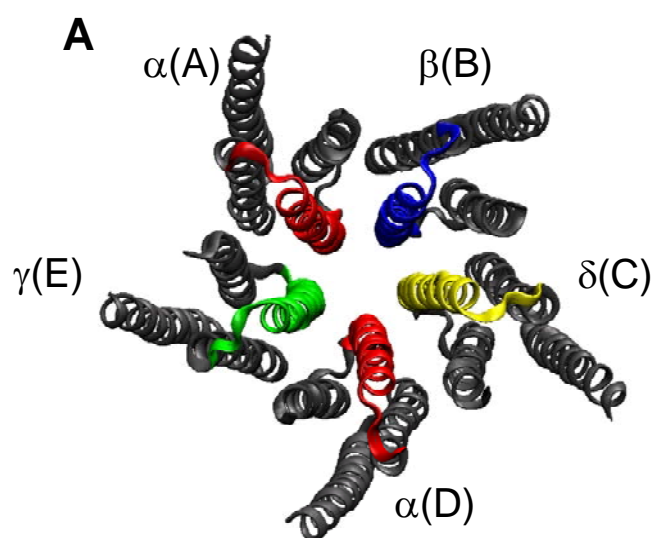
Figure 9:

Porcupine plots of the lowest frequency normal modes acquired from anisotropic network model (ANM) analysis for the 1OED (**A,B**) and an MD structure from a snapshot at 10ns (**C**). **A** Mode 7 for 1OED, seen from the extracellular end of the bundle; **B** Mode 7 for chain α (A)

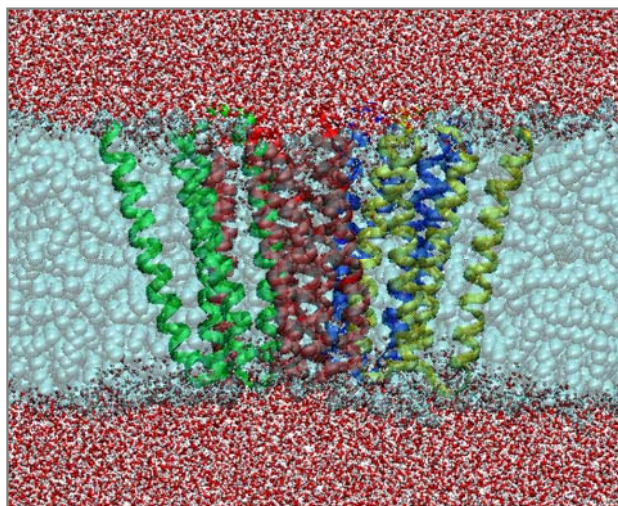
of 1OED viewed perpendicular to the pore axis; **C** Mode 7 for chain $\alpha(A)$ of the MD simulation snapshot. In B,C the hinge point in the M2 helix is indicated by an arrow. (Note that in all of these diagrams only helices M1 to M3 are shown, as the M4 helices were omitted from the ANM analysis – see Methods).

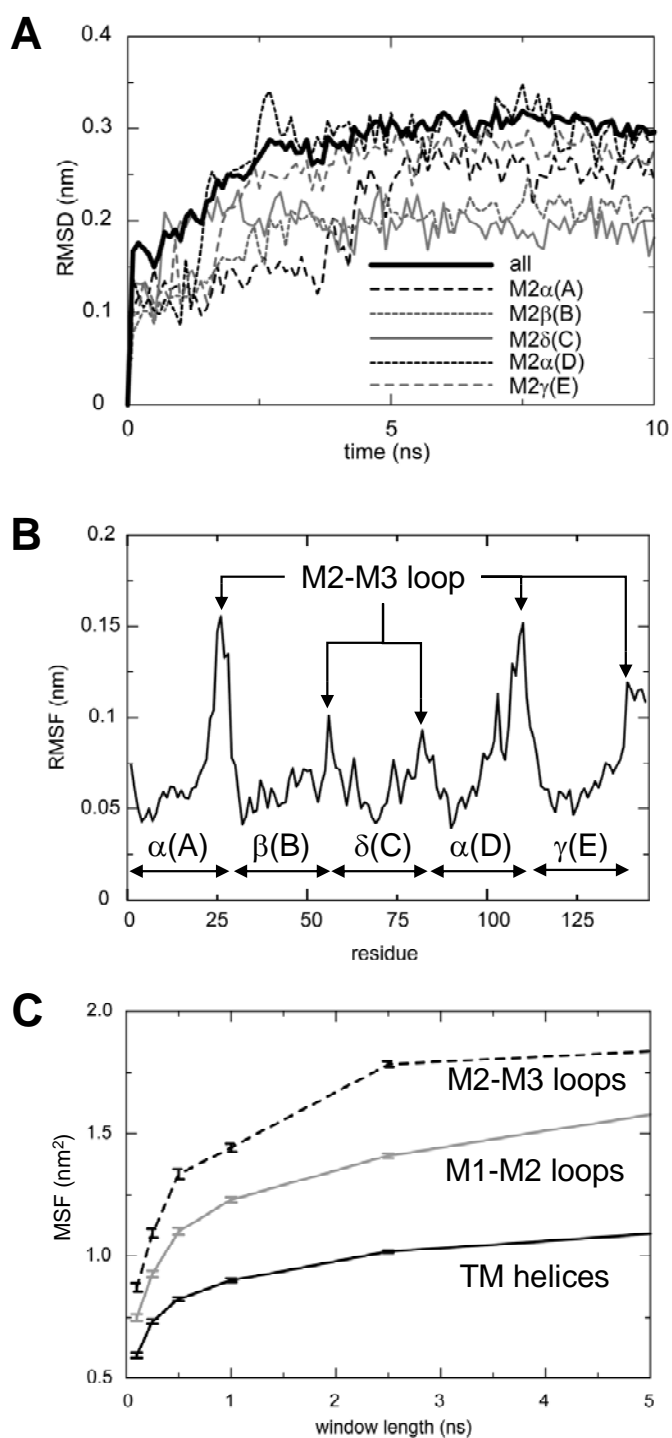
Hung et al., Fig. 1

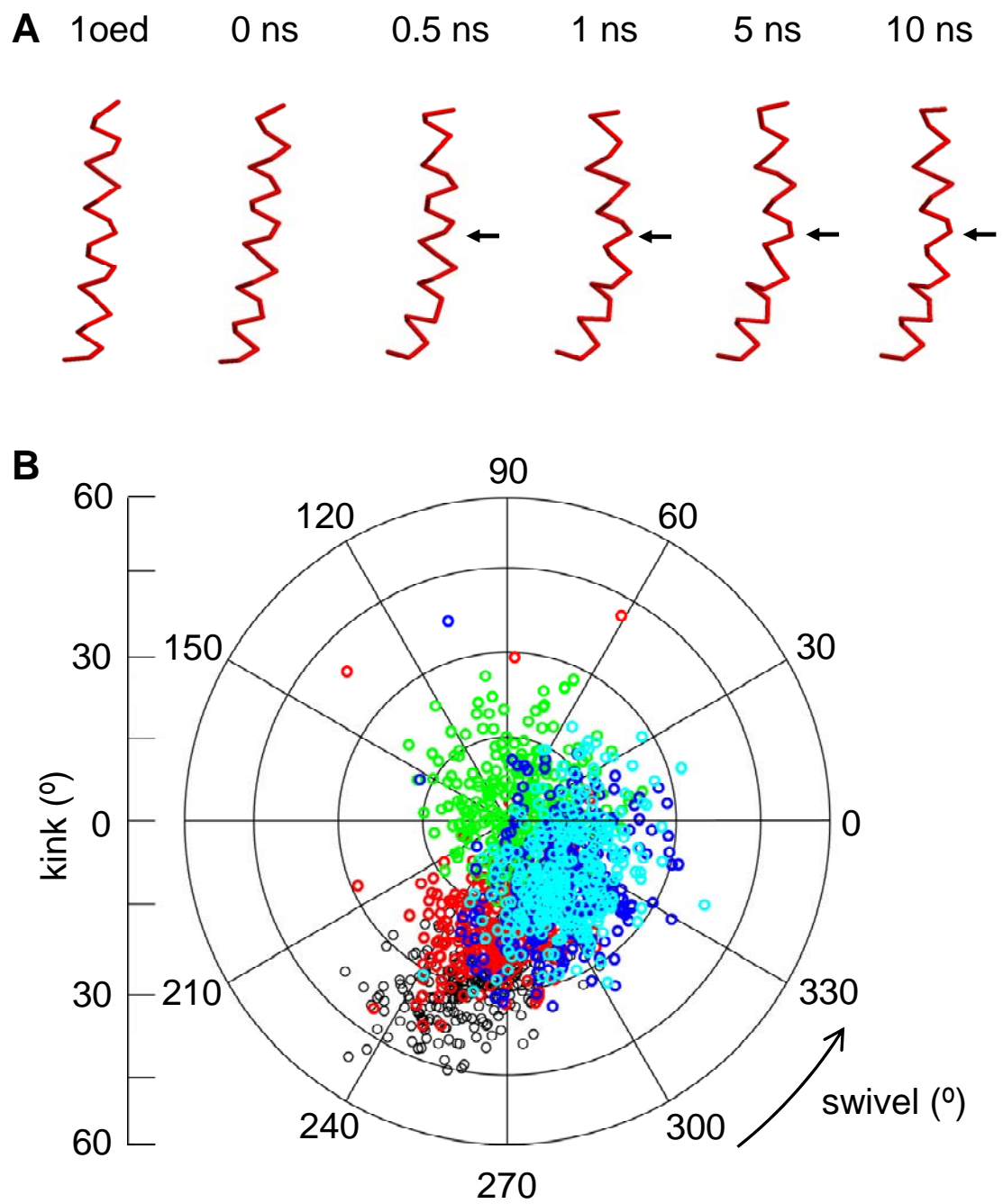
M2 α (A) :	KMTLSISVLL L SLTV <u>F</u> LLVIVELIPSTSSAV
M2 β (B) :	KMSLSISALL L AVTV <u>F</u> LLLLADKVPETSLSV
M2 δ (C) :	KMSTAISVLL L AQAV <u>F</u> LLLTSQLPETALAV
M2 α (D) :	KMTLSISVLL L SLTV <u>F</u> LLVIVELIPSTSSAV
M2 γ (E) :	QKCTLSISVLL L AQT <u>I</u> FLFLIAQKVPETSLNV
	9' 13'

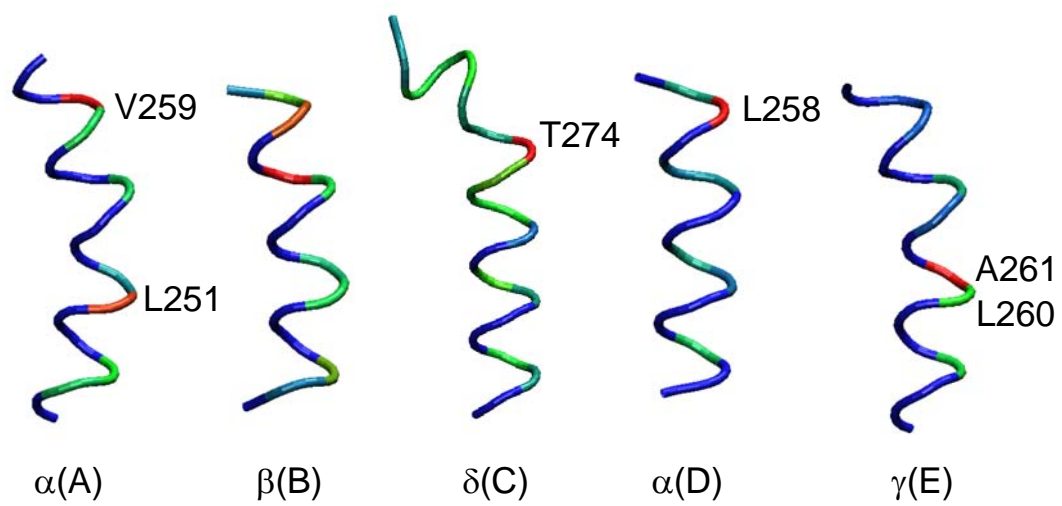


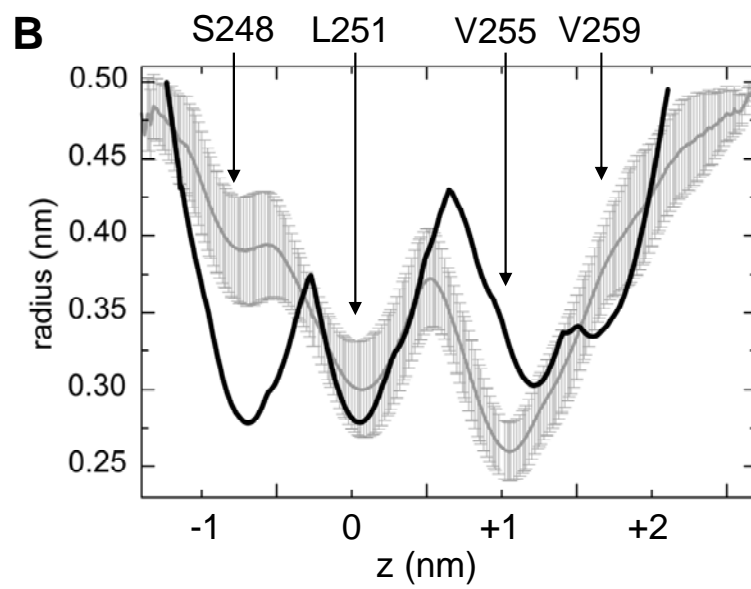
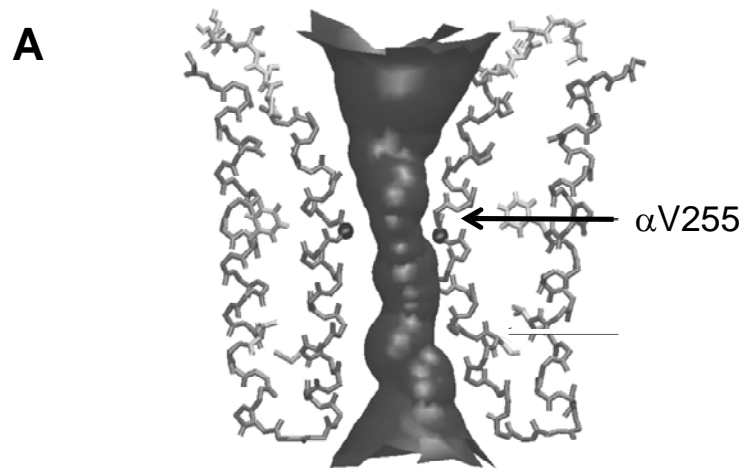
B

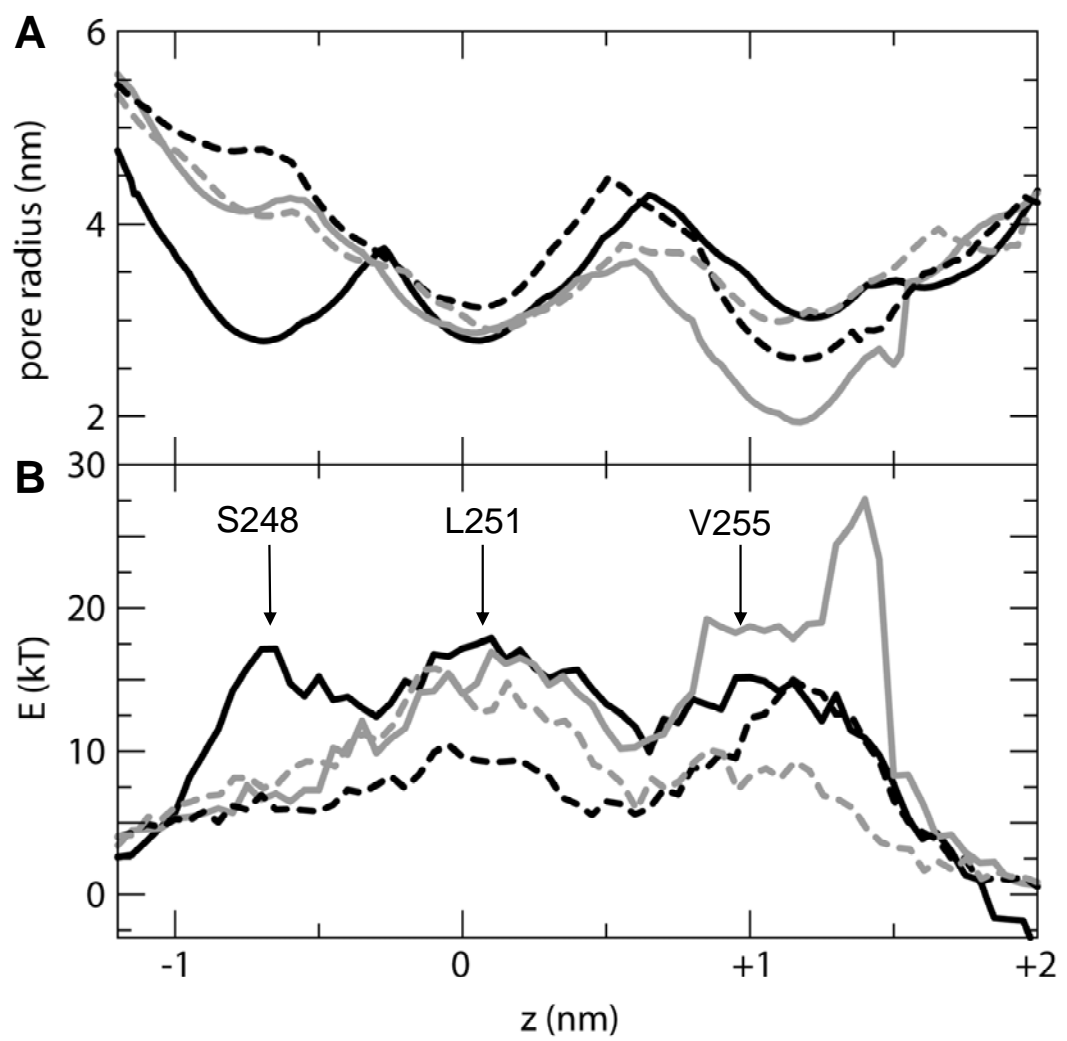












Hung et al., Fig. 8

